[13]M. L. Seman and L. M. Branscomb, Phys. Rev. 125, 1602 (1962).
[14]R. S. Berry, C. W. Reimann, and G. N. Spokes, J. Chem. Phys. 37, 2278 (1962).
[15]R. S. Berry and C. W. Reinmann, J. Chem. Phys. 38, 1540 (1963).
[16]For the most recent H^- calculations, see Refs. 17-19; for the most recent O^- calculations, see Refs. 20-21; for C^-, see Ref. 22.
[17]N. A. Doughty, P. A. Fraser, and R. P. McEachran, Monthly Notices Roy. Astron. Soc. 132, 255 (1966).
[18]S. Geltman, Astrophys. J. 136, 935 (1962).
[19]T. L. John, Monthly Notices Roy. Astron. Soc. 121, 41 (1960).
[20]R. J. W. Henry, Phys. Rev. 162, 56 (1967).
[21]W. R. Garrett and H. T. Jackson, Jr., Phys. Rev. 153, 28 (1967).
[22]V. P. Myerscough and M. R. C. McDowell, in Proceedings of the Sixth International Conference on Ionization Phenomena in Gases, Paris, 1963, edited by P. Hubert and E. Crémieu-Alcan (European Atomic Energy Community, 1964), Vol. I, p. 135.
[23]E. J. Robinson and S. Geltman, Phys. Rev. 153, 4 (1967).
[24]B. Steiner, M. L. Seman, and L. M. Branscomb, Atomic Collision Processes, edited by M. R. C. McDowell (North-Holland Publishing Co., Amsterdam, 1964) p. 537.
[25]J. L. Hall, E. J. Robinson, and L. M. Branscomb, Phys. Rev. Letters 14, 1013 (1965).
[26]S. Geltman, Phys. Letters 4, 168 (1963).
[27]B. Steiner, M. L. Seman, and L. M. Branscomb, J. Chem. Phys. 37, 1200 (1962).
[28]J. Cooper and R. N. Zare, J. Chem. Phys., 38, 942 (1968).
[29]J. L. Hall and M. W. Siegel, J. Chem. Phys., 38, 945 (1968).
[30]Albert Septier, CERN Report No. CERN 60-39, 1960 (unpublished).
[31]P. Mahadevan, G. D. Magnuson, J. D. Layton, and C. E. Carlson, Phys. Rev. 140, A1407 (1965).
[32]The aperture of the optics as determined by external angle was $f/1.2$; the aperture as determined by light-collecting solid angle was $f/1.5$.
[33]J. H. E. Mattauch, W. Thiele, and A. H. Wapstra, Nucl. Phys. 67, 1 (1965).

Hyperfine Contact Interactions in Oxygen Calculated by Many-Body Theory

Hugh P. Kelly
Department of Physics,
University of Virginia,
Charlottesville, Virginia
(Received 15 April 1968)

Many-body perturbation theory, which has been used in previous atomic calculations, is applied to the calculation of the hyperfine contact interaction in the oxygen atom. Large cancellations have been found to occur between different types of diagrams. Both core polarization diagrams and also diagrams representing electron correlations have been found to contribute significantly. The final value for $|\Psi(0)|^2$ is in good agreement with that measured by Harvey.

I. INTRODUCTION AND REVIEW

Many-body perturbation theory, as developed by Brueckner[1] and Goldstone,[2] has been applied to the calculation of many atomic properties such as correlation energies, polarizabilities, and shielding factors.[3-6] The same methods developed to calculate these properties are used in a straightforward manner in this work to calculate the hyperfine contact interaction in the oxygen atom. These methods have also been used recently to calculate the hyperfine contact interaction of the lithium atom.[7]

The contribution of the Fermi contact hyperfine term to the Hamiltonian is given by[8]

$$2\mu_I\mu_0 \sum_{i=1}^{N} \frac{8\pi}{3}\delta(\vec{r}_i)\vec{s}_i\cdot\vec{I}, \tag{1}$$

where μ_I is the nuclear magnetic moment, μ_0 is the Bohr magneton $e\hbar/2mc$, and $\vec{I}$ is the nuclear spin. The first-order contribution of Eq. (1) to the energy may be obtained by evaluating

$$\langle\psi_0|\sum_{i=1}^{N} s_{zi}\,\delta(\vec{r}_i)|\psi_0\rangle/\langle\psi_0|\psi_0\rangle \tag{2}$$

for the ground-state wave function $|\psi_0\rangle$ which is an eigenstate of L^2, S^2, L_z and S_z with eigenvalues $M_L = +L$ and $M_S = +S$. Introducing the normalized state $|LS, M_S = S\rangle = |\psi_0\rangle/(\langle\psi_0|\psi_0\rangle)^{1/2}$, we can relate Eq. (2) to the reduced matrix element[9]

$$\langle LS||\textstyle\sum_i \delta(\vec{r}_i)\vec{s}_i||LS\rangle = \langle LS, M_S = S|\sum_i \delta(\vec{r}_i)s_{zi}|LS, M_S = S\rangle \times \sqrt{3}/(SSS - S|SS10), \tag{3a}$$

where $(SSS - S|SS10)$ is a Clebsch-Gordan coefficient.[9] For oxygen, which has a ^3P ground state ($L = 1, S = 1$), this coefficient is $2^{-1/2}$.

We may also relate Eq. (2) and Eq. (3a) to the quantity

$$|\psi(0)|^2 = \left\langle LS \| \sum_{i=1}^{N} \delta(\vec{r}_i) s_i \| LS \right\rangle \Big/ \langle LS \| \vec{S} \| LS \rangle, \quad (3b)$$

which has been obtained in the experiment of Harvey.[10] For oxygen ($S=1$), $|\psi(0)|^2$ equals Eq. (2).

The state $|\psi_0\rangle$ is the exact solution of the Schrödinger equation.

$$H\psi_0 = E\psi_0, \quad (4)$$

$$\text{with } H = \sum_{i=1}^{N} \left(-\frac{\nabla_i^2}{2} - \frac{Z}{r_i} \right) + \sum_{i<j=1}^{N} r_{ij}^{-1}. \quad (5)$$

(Atomic units are used throughout this paper.)

A first approximation to ψ_0 may be obtained[2] by replacing the many-electron term $\sum_{i<j} r_{ij}^{-1}$ by $\sum_{i=1} V(r_i)$. Then $|\psi_0\rangle$ is approximated by $|\Phi_0\rangle$ and E by E_0, where $|\Phi_0\rangle$ is a determinant containing the N single-particle states φ_n which are the lowest energy solutions of

$$\left[-\frac{\nabla^2}{2} - \frac{Z}{r} + V(r) \right] \varphi_n = \epsilon_n \varphi_n. \quad (6)$$

These are called unexcited states. The unperturbed energy $E_0 = \sum_{i=1}^{N} \epsilon_i$. From the linked-cluster perturbation theory of Brueckner[1] and Goldstone,[2]

$$\psi_0 = \sum_L \{ [1/(E_0 - H_0)] H' \}^n \Phi_0, \quad (7)$$

where $\sum_L$ means that only "linked" terms are to be included. The perturbation

$$H' = \sum_{i<j=1}^{N} r_{ij}^{-1} - \sum_{i=1}^{N} V(r_i). \quad (8)$$

The energy correction

$$\Delta E = E - E_0 = \sum_{L'} \langle \Phi_0 | H' \left(\frac{1}{E_0 - H_0} H' \right)^n | \Phi_0 \rangle, \quad (9)$$

where L' restricts the sum to those terms which are "linked" when the leftmost H' interaction is removed for $n \geq 1$. Perturbation calculations are carried out with a complete set of single-particle states obtained from Eq. (6).

The Brueckner-Goldstone (BG) expansion was previously applied to oxygen to obtain the correlation energy among all pairs of electrons.[5] In Ref. 5 it was pointed out that the state $|\psi_0\rangle$ will be an eigenstate of L^2, S^2, L_z and S_z, if $|\Phi_0\rangle$ is an eigenstate of these operators, and if $\vec{L}$ and $\vec{S}$ commute with $\sum_i V(r_i)$. Use of perturbation theory then avoids the difficulties associated with a method such as the unrestricted Hartree-Fock approximation[11] in obtaining eigenstates of angular momentum.

In Ref. 5 it was observed that Φ_0 for the ground state of many open-shell atoms may be represented by a single determinant provided $M_L = \pm L$ and $M_S = \pm S$. It was also shown that the BG expansion could be extended to the case where Φ_0 is a linear combination of determinants. More general discussions of the linked-cluster expansion for degenerate states are given by Brandow[12] and by Sandars.[13] Sandars[13] has also given an extensive discussion of the use of perturbation theory to calculate hyperfine structure.

In order to calculate Eq. (2) we could calculate ψ_0 by Eq. (7) and then evaluate Eq. (2) directly. In this approach, we remember that $\langle \Phi_0 | \psi_0 \rangle = 1$ and that $\langle \psi_0 | \psi_0 \rangle \neq 1$; so there is a normalization contribution from the denominator of Eq. (2). This is essentially the approach used in a previous calculation of the dipole polarizability of beryllium, where a diagrammatic expression for Eq. (2) was discussed.[4] In this case there is some cancellation of disconnected diagrams for the numerator with normalization terms in the denominator. Another approach,[14] which is probably preferable, is to note that Eq. (2) is equivalent to the sum of all energy diagrams as given by Eq. (9) in which there is one and only one interaction with $\sum_{i=1}^{N} \times s_{zi} \delta(\vec{r}_i)$ and any number of interactions with H' given by Eq. (8). This is the method used in this paper, and all values for diagrams listed in this paper refer to this method of calculation of Eq. (2). In other words, one considers a multiple perturbation calculation[4,6] where H' in Eq. (9) is given by Eq. (8) *plus* $\sum_{i=1}^{N} s_{zi} \delta(\vec{r}_i)$. In calculating polarizabilities one may also use a multiple perturbation expansion in which all energy diagrams with two interactions with the external field are calculated.[6]

II. CALCULATIONS

A. Second-Order Contributions

In evaluating the diagrams contributing to Eq. (2), single-particle states from the previous correlation-energy calculation for oxygen were used. As discussed in Ref. 5, φ_{2s} and φ_{2p} are Hartree-Fock states, and the excited $l=1$ excited states correspond to $2p$ excitations. Since the Hartree-Fock (HF) equation for φ_{2s} was used to calculate all $l=0$ states, φ_{1s} differs by a very small degree from the $1s$ HF solution. For example, $R_{1s}(0) = 43.1308$ as compared with the HF value $R_{1sHF}(0) = 43.1551$. These differences are extremely small and are estimated as negligible in the present calculation. This is also borne out by the calculations of Ref. 5. As discussed in Ref. 5 (see Eq. 31), there is approximately a 5% difference between ϵ_{1s} and the Hartree-Fock ϵ_{1s}. However, when we consider the insertions on hole lines, ϵ_{1s} is shifted to become almost exactly the Hartree-Fock value.[5] The shifted value for ϵ_{1s} is used in the calculations of this paper. Insertions on hole lines also split ϵ_{1s}^+ and ϵ_{1s}^- as well as $\epsilon_{2s}^{\pm}$ as explained later in this section.

In calculating diagrams, sums over bound states are carried out by summing over discrete excitations up to a large value of the principal quantum number and then estimating the remaining infinite sum by the the n^{-3} rule.[4] The sums over continuum states are evaluated by numerical integration.[3,4]

For oxygen with paired $1s^{\pm}$ and $2s^{\pm}$ electrons, the first-order value for Eq. (2) is zero, and the lowest-order contributions are the second-order diagrams

as shown in Fig. 1(a), (b), (c), and (d). The symbols αs may be $1s^+$, $1s^-$, $2s^+$, or $2s^-$. (Generally we use α to represent the entire state. For convenience we sometimes use the more explicit notation αs or $\alpha s^{\pm}$.) By $1s^{\pm}$ we mean a $1s$ electron with $m_S = +1/2$ or $-1/2$. In Fig. 1(a), a $1s$ or $2s$ electron is excited into states ks by interaction with the term $-V$ in the perturbation H' of Eq. (8). The symbol at the top represents the operator $s_z\delta(\vec{r})$. The hyperfine notation is that given by Sandars.[13] In Fig. 1(b) there is a direct interaction with a passive unexcited state and Fig. 1(c) contains an exchange interaction. When a completely unrestricted Hartree-Fock potential is used, diagrams 1(a), (b), and (c) cancel. However, in general, for open-shell atoms one starts from a restricted HF potential, or at least a potential which is independent of m_S; and diagrams 1(a), (b), and (c) do not cancel. Since Φ_0 is the ^3P state of oxygen with $M_L = L$ and $M_S = S$, there are three $2p$ electrons with $m_S = +\frac{1}{2}$ ($m_l = +1, 0, -1$) and one $2p$ electron with $m_S = -\frac{1}{2}$ ($m_l = +1$). Both ϕ_{2s+} and ϕ_{2s-} and also ϕ_{1s+} and ϕ_{1s-} were calculated with exchange interactions with two $2p$ electrons. However, ϕ_{2s+} and ϕ_{1s+} have exchange interactions with three $2p$ electrons while ϕ_{2s-} and ϕ_{1s-} have exchange interactions with one $2p$ electron. The net cancellation of diagrams 1(a), (b), and (c) is given by diagram 1(c) when $\alpha s = 1s^+$ or $2s^+$ and is given by minus the diagram of Fig. 1(c) when $\alpha = 1s^-$ or $2s^-$. For $1s$ states, there are extremely small corrections to this cancellation as discussed in Ref. 5, since ϕ_{1s} is not exactly a HF solution. These corrections are not significant in the calculations of this paper. The diagrams for $2s^+$ and $2s^-$ will add since the top interaction $s_z\delta(\vec{r})$ will also be of opposite sign for $2s^+$ and $2s^-$, and similarly for $1s^+$ and $1s^-$. The diagrams of Fig. 1(a), (b), and (c) also occur inverted as shown in Fig. 1(d). Diagrams 1(a), (b), (c), and (d) are the lowest-order contributions to "core polarization" discussed by Watson and Freeman.[11] For $\alpha = 2s^+$, the diagram of Fig. 1(c) is given, for example, by

$$-\sum_k \tfrac{1}{2}\phi_{2s}(0)\,\phi_{ks}(0)\langle 2p\ ks\,|v|\,2s\ 2p\rangle/(\epsilon_{2s}-\epsilon_k). \tag{10}$$

The summation is over both bound and continuum excited states. Note that in the diagrams k refers to all excited states, both bound and continuum. The contribution of diagrams 1(a) to (d) are summarized in Table I. In Table I, k refers to continuum states and n refers to bound excited states. The results $2s \to k, n$ are obtained by multiplying Eq. (10) by 4 which includes a factor two for the two $2s$ electrons and a factor 2 for the inverted diagrams. A breakdown of the $2s \to n$ contributions of Table I is given in Table II. Most of the result comes from $2s \to 3s$ excitations. In Table I it is seen that the $1s$ and $2s$ contributions nearly cancel.

We may also include the effects of insertions on hole lines of the type shown in Fig. 1(e), where the crossed interaction is meant to include the net effect of the interaction with the potential $-V$ and with all passive unexcited states. These interactions in higher orders may be summed geometrically,[4,5] and the result is a shift in the single-particle energies given by

$$\epsilon_{2s}{}^{\pm} = \epsilon_{2s} \pm \langle 2s2p\,|\,V\,|2p2s\rangle \tag{11}$$

For $\epsilon_{1s}{}^{\pm}$, there is the shift $\mp\langle 1s\ 2p\,|\,V\,|2p\ 1s\rangle$ as well as the shift which causes ϵ_{1s} to become almost exactly the Hartree-Fock value for ϵ_{1s} as shown by Eq. (31) of Ref. 5. Energies of excited states are also shifted similarly to account for insertions on the particle lines as in Fig. 1(e). For excited continuum states, these effects were calculated as described in Ref. 5 and were small compared to the shift of Eq. (11). The result of including these insertions for $2s$ diagrams is given in Table III. There are now significant differences in the $2s^+$ and $2s^-$ contributions, mostly due to the shift of Eq. (11). However, the sum is only slightly different from the $2s$ result given in Table I.

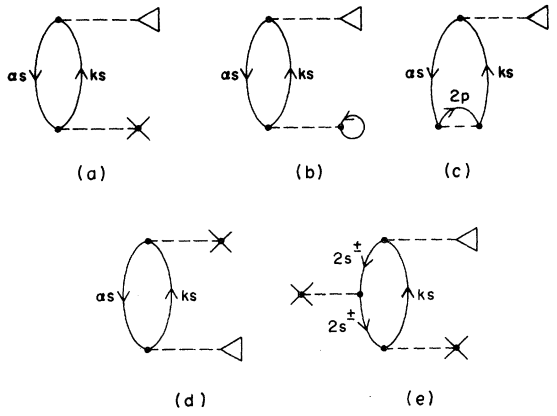

FIG. 1. Lowest-order contributions to Eq. (2). These diagrams represent core polarization effects. The triangular symbol indicates the hyperfine operator $s_z\delta(\vec{r})$. Diagrams (a), (b), and (c) also occur inverted as shown in (d). (e) insertion on the hole line. These modify the single-particle energies.

B. Third-Order Core-Polarization Contributions

In the next order of perturbation theory, we start by considering the modifications to the lowest-order core-polarization diagrams of Fig. 1. These

TABLE I. Lowest-order contributions to Eq. (2).

Excitation	Contribution
$2s \to k$	0.167 77[a]
$2s \to n$	0.056 11[b]
$1s \to k$	−0.205 03[a]
$1s \to n$	−0.006 27[b]
Total	0.012 58

[a] Contribution from continuum excited states.

[b] Contribution from bound excited states.

TABLE II. Bound-state contributions.

n	$2s \rightarrow ns$
3	0.039 08
4	0.008 75
5	0.003 36
6	0.001 64
7	0.000 92
8	0.000 57
$\sum_{n=9}^{\infty}$	0.001 79
Total	0.056 11

diagrams have an additional Coulomb interaction and are shown in Fig. 2. For each diagram shown there is also the inverted diagram obtained by rotating the diagram about a horizontal line through the center. Corresponding to Fig. 2(b) there is also a diagram with the hyperfine interaction and the crossed interaction exchanged. The crossed interactions in Fig. 2 now correspond to interactions with passive unexcited states as well as with $-V$. This notation will be used from now on in this article in all figures other than Fig. 1 in order to save space. In Fig. 2(a) and (b), both hole lines refer to $2s$ states or to $1s$ states since all other diagrams cancel. That is, let the top hole line in Fig. 2(a) refer to $2s^+$. Then, there is an equal and opposite contribution according to whether the bottom hole line is $1s^+$ or $1s^-$. As a result, only the exchange diagrams contribute when one hole line is $2s$ and the other is $1s$, as shown in Fig. 2(c), (d), and (e). Similarly, only exchange diagrams contribute when one hole line is $2s$ or $1s$ and the other is $2p$. That is, all the direct diagrams add to zero in these cases except for 2(a) and 2(b). We note that the net interaction of $2p$ ($m_l = +1$, $m_S = -\frac{1}{2}$) with the other unexcited states and with $-V_{\mathrm{HF}}$ is equal and opposite to the sum of this net interaction for the three other $2p$ electrons with $m_S = +\frac{1}{2}$.

TABLE III. $2s$ contributions with insertions of Fig. 1(e).

Excitation	Contribution[a]
$2s^+ \rightarrow k^+$	0.078 82[b]
$2s^+ \rightarrow n^+$	0.024 65[c]
$2s^- \rightarrow k^-$	0.089 49[b]
$2s^- \rightarrow n^-$	0.032 50[c]
Total	0.225 46

[a] $\epsilon_{2s^+} = -1.401\,87$, $\epsilon_{2s^-} = -1.087\,11$. Insertions on particle lines also included.

[b] Continuum excitations.

[c] Bound-state excitations.

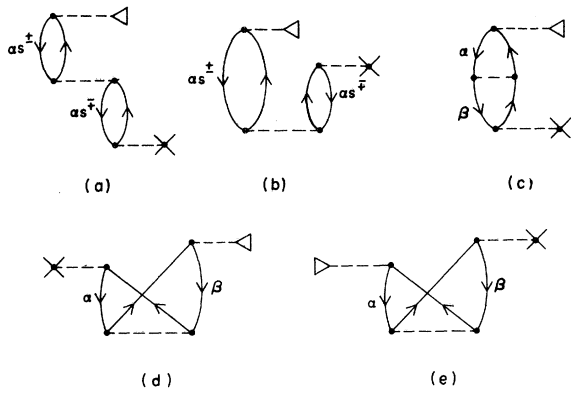

FIG. 2. Third-order core polarization diagrams. These diagrams are second order in the Coulomb interactions and first order in the hyperfine interaction that is represented by the triangular symbol. The crossed interaction represents the net effect of interactions with $-V$ and with all passive unexcited states. There are also inverted diagrams corresponding to all diagrams shown. There is also a diagram like (b) with the crossed interaction and the hyperfine interaction interchanged.

The numerical contributions of the diagrams of Fig. 2 are given in Table IV. Inverted diagrams are included in the results and also the diagram like Fig. 2(b) but with the top two interactions interchanged. The total contribution of diagrams 2(a) and 2(b) with $\alpha = 2s$ is 0.031 98. Of this value, 0.019 49 comes from the case when both excited

TABLE IV. Contributions from diagrams of Fig. 2.

Diagram	Value[a]
(a) $\alpha s = 2s$	0.015 99
(b) $\alpha s = 2s$	0.015 99[b]
(a) $\alpha s = 1s$	−0.006 01
(b) $\alpha s = 1s$	−0.006 01[b]
(c) $\alpha = 2s^{\pm}$, $\beta = 1s^{\pm}$	−0.001 17
(c) $\alpha = 1s^{\pm}$, $\beta = 2s^{\pm}$	0.009 25
(d) $\alpha = 1s^{\pm}$, $\beta = 2s^{\pm}$	−0.000 63
(d) $\alpha = 2s^{\pm}$, $\beta = 1s^{\pm}$	0.000 31
(e) $\alpha = 1s^{\pm}$, $\beta = 2s^{\pm}$	0.008 54
(e) $\alpha = 2s^{\pm}$, $\beta = 1s^{\pm}$	−0.000 24
(c) $\alpha = 2s^{\pm}$, $\beta = 2p^{\pm}$	0.022 87
(d) $\alpha = 2p^{\pm}$, $\beta = 2s^{\pm}$	0.003 21
(e) $\alpha = 2s^{\pm}$, $\beta = 2p^{\pm}$	0.006 41
(c) $\alpha = 1s^{\pm}$, $\beta = 2p^{\pm}$	−0.005 97
(d) $\alpha = 2p^{\pm}$, $\beta = 1s^{\pm}$	−0.000 02
(e) $\alpha = 1s^{\pm}$, $\beta = 2p^{\pm}$	−0.005 12
Total	0.057 40

[a] The inverted diagrams are also included. The crossed interaction in Fig. 2 represents the net interaction with $-V$ and with all passive unexcited states.

[b] The diagram with the hyperfine interaction and the crossed interaction exchanged is also included.

states are in the continuum. When one excited state is bound and the other is in the continuum, the result is 0.010 91; and when both excited states are bound, the result is 0.001 58. As is expected from Table I, the bound excited states are less important for Fig. 2(a) and (b) when $\alpha = 1s$. In this case, the total is $-0.012\,02$, with $-0.011\,53$ contributed from two continuum excitations. In Fig. 2(c) with $\alpha = 2s^{\pm}$, and $\beta = 1s^{\pm}$ the excitations with at least one bound state contribute 8.1% of the total. For diagram 2(c) with $\alpha = 1s^{\pm}$, $\beta = 2s^{\pm}$, excitations with at least one bound state contribute 25% of the total. It is seen that although two continuum excitations give the largest contributions, bound-state excitations are still quite significant.

C. Correlation Diagrams

We now consider diagrams which do not depend on core polarization but depend on true correlation effects. The basic diagrams are shown in Fig. 3 and the contributions of these diagrams are listed in Table V. The largest values are contributed by diagrams 3(a) and its exchange 3(b), including the diagram like (b) where the labeling on the particle lines is interchanged. The contribution from 3(a) when $\alpha = \beta = 2s^{-}$ is seen to be very large. This is not surprising since similar excitations were found to be very large in the previous correlation-energy calculations.[5] The value 0.066 31 was calculated using shifted denominators to account for insertions on the hole and particle lines as discussed in connection with Eq. (11). These shifts also accounted for hole-particle and ladder diagrams as discussed in the correlation energy calculations.[5] Nevertheless, the net effect of including such higher-order terms in connection with diagram 3(a) is not large, since the result without any shifts is 0.065 54. The nondiagonal ladder diagrams for 3(a) were calculated and also found to be small, and they are not included. A rough estimate indicates a contribution of -0.0020 from the nondiagonal ladder diagrams.

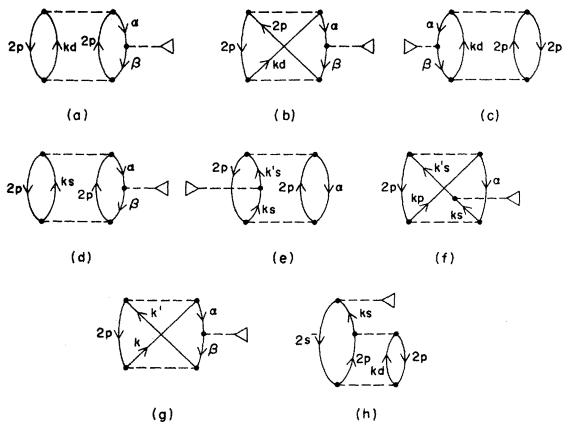

FIG. 3. Correlation diagrams. All particle lines labeled $2p$ refer to the excited $2p$ state with $m_S = -\frac{1}{2}$ and $m_l = 0$ and -1. The excited $2p$ states are not included in kp. Diagrams (b), (f), and (g) with the particle lines interchanged should also be included.

TABLE V. Contributions from diagrams of Fig. 3.

Diagram	Value
(a) $\alpha = \beta = 2s^{-}$	0.066 31[a]
(b) $\alpha = \beta = 2s^{-}$	−0.020 19[b]
(a) $\alpha = \beta = 1s^{-}$	0.001 67
(b) $\alpha = \beta = 1s^{-}$	−0.000 41[b]
(a) $\alpha = 1s$, $\beta = 2s$	−0.007 23
(a) $\alpha = 2s$, $\beta = 1s$	−0.007 23
(b) $\alpha = 1s$, $\beta = 2s$	0.001 07[b]
(b) $\alpha = 2s$, $\beta = 1s$	0.002 07[b]
(c) $\alpha = \beta = 2s^{\pm}$	0.001 00[c]
(d) $\alpha = \beta = 2s^{-}$	0.002 89
(d) $\alpha = 1s^{-}$, $\beta = 2s^{-}$	−0.001 02[b]
(d) $\alpha = \beta = 1s^{-}$	0.000 20
(e) $\alpha = 2s^{-}$	0.001 38
(e) $\alpha = 1s^{-}$	0.000 06
(f) $\alpha = 2s$	−0.011 26
(f) $\alpha = 1s$	0.000 62
(g) $\alpha = \beta = 2s$	0.009 92[d]
(g) $\alpha = 1s$, $\beta = 2s$	−0.003 62[b, d]
(g) $\alpha = \beta = 1s$	0.000 59[d]
(h)	−0.020 44
Total	0.016 38

[a] Shifted denominators used. Without the shifts, the result is 0.065 54.
[b] Inverted diagrams included. For (b), this means interchange labels on the particle lines.
[c] Shifted denominators included so there is not exact $2s^{+}$, $2s^{-}$ cancellation.
[d] $l = 0$, 1, and 2 excitations included.

In all diagrams, the continuum excitations gave the largest contributions with bound-state effects also large for $l = 0$ and $l = 1$ bound excited states. However, the $l = 2$ bound excited states contributed only small amounts. For diagram 3(a) with $\alpha = \beta = 2s^{-}$, the bound states contributed 0.000 88 which is 1.3% of the total. However, in diagram 3(k) the continuum excitations contribute $-0.012\,97$ and $l = 0$ bound excited states contribute $-0.007\,06$. Exchange diagrams for Fig. 3(h) and higher iterations of the single excitation at the top of Fig. 3(h) by interactions of the types of Fig. 2 are estimated to nearly cancel and are not listed. We also note that there is much cancellation among the different contributions listed in Table V. For example, the results from diagrams 3(d) and 3(e) are approximately equal and opposite to the results from diagrams 3(f) and 3(g).

D. Higher-Order Diagrams

Some of the types of higher-order diagrams which have been considered are shown in Fig. 4, and the results of calculating them are listed in Table VI. The diagrams 4(a), (b), (c), and (d) are typical higher-order iterations of the diagrams of Fig. 2. All possible iterations of the basic diagrams of Fig. 2 were considered, not only 4(a) to (d). Reliable

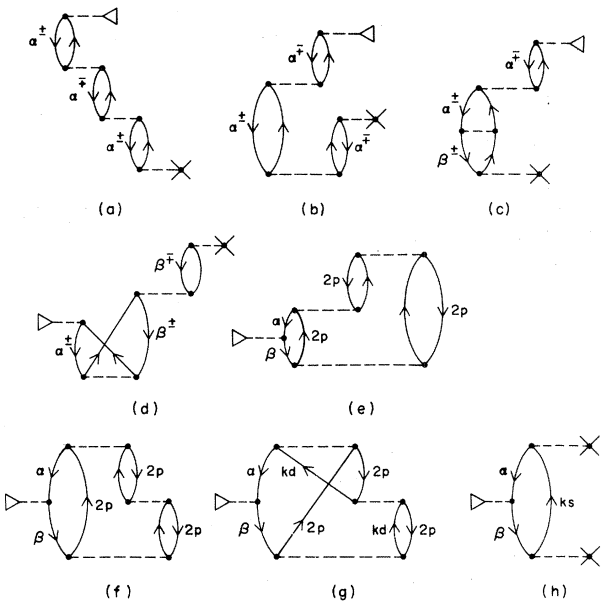

FIG. 4. Typical higher-order diagrams. (a), (b), (c), and (d) are typical higher-order iterations of the diagrams of Fig. 2. (a) and (b) involve only two different unexcited states. (c) and (d) involve three different unexcited states. Diagrams (e), (f), and (g) correspond to the lowest-order three-body correlation energy diagrams with two $2p$ hole states and $2s$ hole states and a $2s^-$ or $1s^-$ electron excited into the $2p$ excited states. (g) is only one example of the possible exchange terms. (h) should be calculated with shifted denominators to account for insertions on the hole line and particle line. In order to reduce the number of figures, the crossed interaction represents the net effect of interactions with $-V$ and also with all passive unexcited states.

estimates of these types of diagrams may often be obtained[4,5] by considering ratios of the diagrams of Fig. 2 to those of Fig. 1. For example, we would estimate the diagram of Fig. 4(a) by multiplying the diagram of Fig. 2(a) by the ratio of 2(A) to 1(a). Diagrams 4(e), (f), and (g), including all possible exchange terms, were directly calculated. Diagrams of Fig. 4(h) were calculated with shifted denominators as in Eq. (11). In 4(h), the excitation k may have either $l=0$ or $l=2$. For $l=0$, the hyperfine interaction may also occur on the particle line and this was included. The total result is extremely small.

Other higher-order terms which were found to contribute large effects are shown in Fig. 5. We call these "renormalization" diagrams, since the effect of these diagrams is to "renormalize" the basic diagram of Fig. 1(a). Diagrams 5(a), (e), (f), (g), and (k) are also called rearrangement diagrams.[15] These same interactions are also repeated in higher orders. In diagrams (e) and (f), the correlation part of the diagram involving n has two different time orderings relative to the basic part of Fig. 1(a). The sum of these two terms is minus diagram 1(a) times the correlation energy of the

TABLE VI. Contributions from diagrams of Fig. 4.

Diagram	Value
(a)—(d)	0.00768[a]
(e), (f), (g); $\alpha=\beta=2s^-$	-0.01861[b]
(e), (f), (g); α or $\beta=1s^-$	0.00303[b]
(h)	0.00037[c]
Total	-0.00753

[a]Estimated result. All possible higher iterations of Fig. 2 included in estimate, not only the examples of Fig. 4. Also includes estimate of all higher orders.

[b]All possible exchange diagrams included, of which Fig. 4(g) is only one example.

[c]Includes a small contribution from case where k has $l=0$ and the hyperfine interaction is on the particle line.

pair n, α divided by the denominator of the 1(a) part. As discussed previously,[4] the higher-order interactions like 5(e) and (f) give a geometrical series which may be summed to give the basic diagram of Fig. 1(a) with a shifted denominator such that

$$\epsilon_\alpha \to \epsilon_\alpha + \sum_{\substack{n=1 \\ (n\neq\alpha)}}^{N} E_c(\alpha,n), \tag{12}$$

where $E_c(\alpha,n)$ is the pair correlation energy for α,n. The sum of diagrams 5(g) and (h) is given by minus diagram 1(a) times

$$Nm(\alpha,n)=\sum_{k,k'}|\langle kk'|v|n\alpha\rangle|^2/(\epsilon_\alpha+\epsilon_n-\epsilon_k-\epsilon_{k'})^2. \tag{13}$$

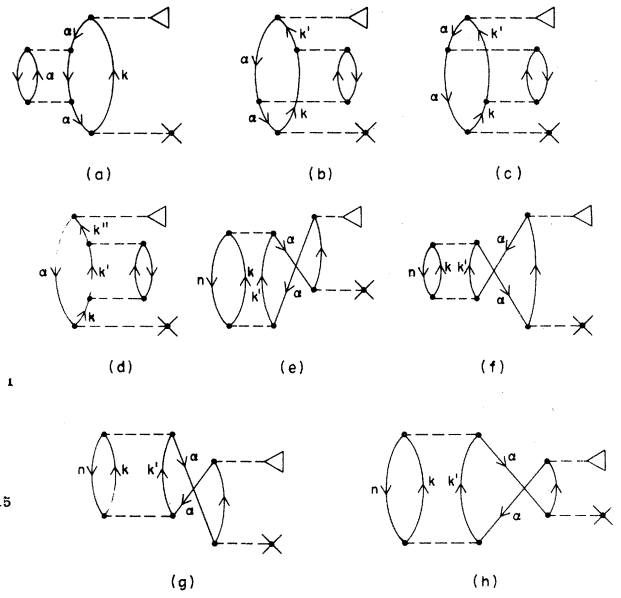

FIG. 5. Renormalization diagrams which modify the basic diagram of Fig. 1(a).

The quantity $Nm(\alpha,n)$ is similar to the pair correlation energy $E_C(\alpha,n)$, except that Nm is calculated with a squared denominator. If we had used Eq. (2) directly to calculate the hyperfine energy, we would have calculated

$$\langle\psi_0|\psi_0\rangle = 1 + \sum_{p<q} Nm(p,q), \tag{14}$$

where $\sum_{p<q}$ is a summation over all pairs of unexcited states (p,q). As previously discussed,[4] there may be much cancellation between $\langle\psi_0|\psi_0\rangle$ and disconnected terms occurring in $\langle\psi_0|O|\psi_0\rangle$, where O is the operator being evaluated. After this cancellation we are effectively left with the diagrams like Fig. 5(g) and (k). Renormalization diagrams are expected to be more important for $\alpha = 2s^{\pm}$ than for $1s^{\mp}$, since denominators in the latter case are much larger. Since the contribution from the diagram of Fig. 1(a) with $\alpha = 2s^{\pm}$ is considerably larger than our final value, we may expect significant effects from the renormalization diagrams of Fig. 5, even though these diagrams are much smaller than Fig. 1(a).

The results of calculating the diagrams of Fig. 5 are listed in Table VII. There is much cancellation among diagrams 5(a), (b), (c), and (d). This is not very surprising when we consider the structure of the diagrams. We note that 5(a) and (d) have the same sign, which is opposite to the sign of 5(b) and 5(c). Diagram 5(a) was calculated to be 0.008 68, but the total of (a), (b), (c), and (d) is 0.002 47. The value for 5(e)+5(f), which is the largest contribution, was obtained by recalculating the diagrams of Fig. 1 with the shift in denominators given by Eq. (12). Values for $\sum_n E_C(2s^{\pm},n)$ were taken from the oxygen correlation energy calculation.[5] Higher-order iterations of 5(e) and 5(f) are then included in the result. In order to obtain $Nm(\alpha,n)$ for diagrams 5(g) and 5(h), the pair correlation energies of Ref. 5 were divided by an average energy denominator which was chosen in each case from the middle of the range of important excitations for the correlation energy. The $1s^{\pm}$ contributions are much smaller as expected. Renormalization effects on the basic diagrams of Figs. 2, 3 (except h), and 4 have been estimated and given in Table VII. Most of this result comes from the diagrams of Fig. 2 and Fig. 4(a)–(d). The renormalization diagrams associated with Fig. 3(h) were omitted because we have estimated a cancellation between the exchange terms of 3(h) and the higher-order terms associated with 3(h). We note that the diagrams of Fig. 5 reduce the basic diagrams of Fig. 1 by 6% when $\alpha = 2s^{\pm}$. However, the relative effect of the renormalization diagrams increases in higher orders. For example, the diagram of Fig. 2(a) for $\alpha = 2s^{\pm}$ is reduced by 12% by the renormalization diagrams.

The final result for the oxygen hyperfine contact interaction as given by Eq. (2) is obtained by adding the total results of Tables I, IV, V, VI, and VII, and then adding the quantity 0.001 58 which accounts for the correction of Table III to the 2s results of Table I. The result is 0.0601.

TABLE VII. Contributions from renormalization diagrams of Fig. 5.

Diagram	Value
(a), (b), (c), (d); $\alpha = 2s^{\pm}$	0.00247
(e), (f); $\alpha = 2s^{\pm}$	−0.01075
(g), (h); $\alpha = 2s^{\pm}$	−0.00534[a]
(a)–(h); $\alpha = 1s^{\pm}$	0.00060
Higher-order terms	−0.00733[b]
Total	−0.02035

[a] Estimated with correlation energy results of Ref. 5.
[b] Estimate of renormalization effects on diagrams of Figs. 2, 3 (except h), and 4.

III. DISCUSSION AND CONCLUSIONS

The calculated value 0.0601 for Eq. (2), or $|\psi(0)|^2$, may be compared with the experimental result of Harvey[10] which is 0.0569. We note that the value 0.0601 calculated in this paper does not include relativistic effects which we would expect to be small. Approximate calculations[16,17] of the relativistic effects for $|\psi(0)|^2$ in oxygen indicates that they are very small. Judd[17] reports a decrease in $|\psi(0)|^2$ by 2% due to relativistic effects. The value for $|\psi(0)|^2$ calculated in this paper may also be compared with the results of Bessis, Lefebvre-Brion, and Moser[18] who calculated the magnetic hyperfine-structure constant a_S $(J=2)$ which, in the case of oxygen, equals $(8\pi\mu_I\mu_0/3I)|\psi(0)|^2$. Bessis *et al.* calculated a_S $(J=2)$ by means of configuration interaction and obtained −11.5 Mc/sec. They performed an unrestricted Hartree-Fock calculation which gave $a_S = -19.5$ Mc/sec, and they also made an extended unrestricted Hartree-Fock calculation which resulted in −34 Mc/sec. Their projected unrestricted Hartree-Fock result for the latter case is −17 Mc/sec, which is in excellent a agreement with the experimental value −17.2 Mc/sec. The result calculated in this paper is −18.2 Mc/sec, not including the relativistic corrections.

In examining the results of the previous section we find very large cancellations between the lowest-order core polarization diagrams of Fig. 1 for 1s and 2s electrons. There are large contributions from the core polarization diagrams in the next order as shown in Fig. 2. These contributions are, however, considerably smaller than the lowest-order results of Fig. 1 for 2s electrons alone. From Table II we also observe that there are large contributions from the core-polarization-type diagrams in which a 2p electron is excited or de-excited through the net interactions with $-V$ and with the other unexcited electrons. These contributions come to 0.032 49 when the other electron which is excited is $2s^{\pm}$ and −0.011 11 when the other electron is $1s^{\pm}$. Even though the third-order diagrams (second order in Coulomb interactions and first order in the hyperfine interactions) of Fig. 2 give a larger net contribution than the second-order terms of Fig. 1, this does not imply a divergence

of the expansion but merely reflects the near cancellation of the second-order terms. In the next order in the Coulomb interaction, the diagrams corresponding to Fig. 4(a)–(d) contribute 0.006 76, which is only 12% of the result from the diagrams of Fig. 2. The value 0.007 68 in Table VI includes an estimate of all higher iterations of these types of interactions. We see that the core polarization effects are large and add to a result which is larger than the experimental value 0.0569. Under "core polarization" we have included all diagrams with at least one interaction with $-V$ and with the unexcited states – as in Figs. 1, 2, 4(a)–(d), and 4(h).

We also find that many diagrams which involve true correlations may be quite large. The most striking example is the diagram of Fig. 3(a) with $\alpha = \beta = 2s^-$. When $\alpha = \beta$, the hole-line interaction is diagonal, and we have an example of an "exclusion-principle-violating diagram." Only $2s^-$ or $1s^-$ electrons may be excited into the $2p$ ($m_S = -\frac{1}{2}$) excited states. When such an excitation occurs, the $2s^+$ or $1s^+$ electron remains unexcited and there is an effective net spin density at the nucleus. Since such excitations were found to be important in the correlation energy calculations,[5] it is not surprising that they play an important role in the present work. However, we note that there is much cancellation among the various correlation diagrams of Fig. 3.

In investigating higher-order terms beyond those of Figs. 2 and 3, we first included the terms of Fig. 4 and listed their contributions in Table VI. The first entry includes all terms like Fig. 4(a)–(d), and also estimates of all higher iterations of these effects. Contributions from the diagrams of Fig. 4(e), (f), and (g) are also listed in Table VI, including all possible exchange diagrams. When the hyperfine interaction is removed, these correspond to the lowest-order three-body correlation energy diagrams with two $2p$ hole states and a $2s^-$ or $1s^-$ electron excited into the $2p^-$ excited states. In Fig. 4(e), (f), and (g) these are also three-body diagrams when $\alpha = \beta$, and are four-body diagrams when $\alpha \neq \beta$. Although the sum of these diagrams is smaller than diagrams such as Fig. 3(a) and (b), which are the corresponding lower-order diagrams, the contributions from Fig. 4(e), (f), and (g) are fairly large. It is not known whether there may be significant contributions from higher-order diagrams such as Fig. 4(e), (f) and (g) which involve the same number of hole lines but more Coulomb interactions. Among these diagrams are those involving triple excitations; and there has been almost no work on the effects of three-particle excitations in the atomic correlation problem, except for a calculation for the hyperfine structure of nitrogen by Nesbet.[19] However, such terms have been considered in the nuclear many-body problem by Bethe.[20] It is possible that the basic three-body diagrams with triple excitations will not add up to a very large result, since for each excitation through interaction with a particle line there is also a possible excitation through interaction with a hole line, and these two types of excitations will be of opposite sign. This is analogous to the situation in Fig. 5 where the double excitation may take place through interaction with a hole line [as in diagrams 5(a) and (b)] or through interaction with a particle line [as in Fig. 5(c) and (d)]. We found that there is a fair degree of cancellation among diagrams 5(a), (b), (c), and (d). In this case, the effects from interaction with the hole line were greater; the same should be true for the three-body diagrams. This would increase the results from Fig. 4(e), (f), and (g) and cause a small reduction in our final result.

Since the basic three-body diagrams of Fig. 4(e), (f), and (g) contribute significantly although they are smaller than diagrams 3(a) and 3(b), we might expect a small but non-negligible contribution from the basic four-body diagrams with one more $2p$ hole line than in Fig. 4(e), (f), and (g). We can make a very rough estimate of these effects by taking the ratio of the direct diagrams of Fig. 4(e) and (f) to Fig. 3(a) with $\alpha = \beta = 2s^-$. Using this ratio of -0.405, we estimate the contribution from basic four-body and five-body terms as roughly 0.003 75. However, this result is expected to be too large, since in the four-body case the number of different exchange diagrams is increased over the three-body case, causing a further reduction. The uncertainty in these four-body and five-body terms, and also in higher-order three-body terms, contributes an uncertainty from 5 to 10% in the calculated result.

It has also been interesting to note the large contributions from the renormalization diagrams of Fig. 5. Much of the importance of these effects is due to the large contributions of Fig. 1 which nearly cancel. However, the renormalization diagrams have a much greater effect on the basic diagrams of Fig. 1 with $\alpha = 2s^\pm$ than on those with $\alpha = 1s^\pm$. This is due to the much larger energy denominators associated with $1s$ excitations, and also due to the fact that the $2s$ electrons have larger correlation effects than the $1s$ electrons.[5] Although the renormalization diagrams contribute very significantly to the final result, they are a small fraction of the second-order contribution from excitations of $2s$ electrons. These renormalization diagrams are also expected to be important in many other calculations.

In addition to those results listed in the tables, the nondiagonal ladder diagrams associated with diagrams like those of Fig. 3 were found to be small (approximately -0.0020) and are not included. Also, in diagrams like Fig. 2(b), where there are two electrons simultaneously excited, in higher orders there are hole-hole, hole-particle, and ladder diagrams as discussed in Ref. 5. The net effect of these diagrams was found[5] to be approximately a 5% reduction of the pair correlation energies. This would lead to an approximate result of $-0.001\,50$ in the present work.

Many different diagrams have been included in this work, and it is hoped that all important diagrams were included. However, there are uncertainties due to the higher-order diagrams which were neglected, and due to those effects which were estimated by partial calculation. The overall estimated uncertainty in the calculated result is approximately 10%.

It is hoped that this work illustrates the usefulness of many-body perturbation theory in atomic hyperfine calculations. The methods developed

previously which have been used in this paper are applicable to other atoms and other atomic properties. However, in other calculations of hyperfine structure we may find that many of the near cancellations of diagrams found in this paper do not occur; and we may also find that other diagrams are important.

ACKNOWLEDGMENTS

I wish to thank Professor K. M. Watson who suggested this problem many years ago. I also gratefully acknowledge very helpful conversations and communications with Professor J. S. M. Harvey, Professor B. R. Judd, Professor C. M. Moser, Professor Wilhelm Pieper, Professor P. G. H. Sandars, and Professor M. Barnhill III. I am grateful to the U. S. Atomic Energy Commission and the National Science Foundation for financial support.

*Work supported in part by the U.S. Atomic Energy Commission, Document ORO-2915-88, and the National Science Foundation.

[1]K. A. Brueckner, Phys. Rev. 97, 1353 (1955); 100, 36 (1955); The Many-Body Problem (John Wiley & Sons, Inc., New York, 1959).
[2]J. Goldstone, Proc. Roy. Soc. (London) A239, 267 (1957).
[3]H. P. Kelly, Phys. Rev. 131, 684 (1963).
[4]H. P. Kelly, Phys. Rev. 136, B896 (1964).
[5]H. P. Kelly, Phys. Rev. 144, 39 (1966).
[6]H. P. Kelly, Phys. Rev. 152, 62 (1966).
[7]E. S. Chang, Ph. D. thesis, University of California at Riverside, 1967, (unpublished).
[8]N. F. Ramsey, Nuclear Moments (John Wiley & Sons, Inc., New York, 1953), p. 10; B. R. Judd, Operator Techniques in Atomic Spectroscopy (McGraw-Hill Book Co., Inc., New York, 1963), p. 85.
[9]A. R. Edmonds, Angular Momentum in Quantum Mechanics (Princeton University Press, Princeton, N.J., 1960), p. 75.
[10]J.S. M. Harvey, Proc. Roy. Soc. (London) A285, 581 (1965).
[11]R. E. Watson and A. J. Freeman, in Hyperfine Interactions, edited by A. J. Freeman and R. B. Frankel (Academic Press Inc., New York, 1967), p. 53.
[12]B. H. Brandow, Rev. Mod. Phys. 39, 771 (1967).
[13]P. G. H. Sandars, in La Structure Hyperfine des Atomes et des Molecules, edited by R. Lefebvre and C. Moser (Editions du Centre National de las Recherche Scientifique, Paris, 1967), p. 111; Advan. Chem. Phys. (to be published).
[14]D. J. Thouless, The Quantum Mechanics of Many-Body Systems (Academic Press Inc., New York, 1961).
[15]K. A. Brueckner and D. T. Goldman, Phys. Rev. 117, 207 (1960).
[16]W. Pieper, unpublished.
[17]B. R. Judd, in La Structure Hyperfine des Atomes et des Molecules, edited by R. Lefebvre and C. Moser (Editions du Centre National de la Recherche Scientifique Paris, 1967), p. 311.
[18]N. Bessis, H. Lefebvre-Brion, and C. M. Moser, Phys. Rev. 128, 213 (1962).
[19]R. K. Nesbet, Advan. Chem. Phys. (to be published).
[20]H. A. Bethe, Phys. Rev. 138, B804 (1965).

Measurement of the Sodium *D*-Line Absolute Oscillator Strengths by the Roschdestvenskii Hook Method

Carl A. Forbrich, Jr.,
U.S. Air Force Academy, Colorado Springs, Colorado
and
Wayland C. Marlow
Lockheed Missiles and Space Company, Palo Alto, California
and
Daniel Bershader
Stanford University, Stanford, California
(Received 24 April 1968)

The absolute oscillator strengths for the sodium *D* lines have been measured using the Roschdestvenskii hook method, a technique which can provide an accurate means for measuring the product of the population and *f* value, *Nf*, for a gas. The experiment was performed under well-defined conditions, with a systematic variation of temperature, fringe angle, and fringe spacing. It was found that the *f* values were independent of these variations in accordance with expectations. The measured *f* values were $f_{D_2} = 0.677 \pm 0.007$ and $f_{D_1} = 0.341 \pm 0.009$. These results are in excellent agreement with the quantum-mechanical calculations which employ Bates-Damgaard or Hartree-Fock methods.

The work presented here represents the first phase of a program to apply spectral interferometry to the study of atomic properties and behavior of shock-heated gases. A well-known and particularly powerful technique in this area is the Roschdestvenskii "hook method," which yields the prod-